

Unwinding the model manifold: choosing similarity measures to remove local minima in sloppy dynamical systems

Benjamin L. Francis¹ and Mark K. Transtrum^{1,*}

¹*Department of Physics and Astronomy, Brigham Young University, Provo, Utah 84602, USA*

(Dated: December 14, 2024)

In this paper, we consider the problem of parameter sensitivity in models of complex dynamical systems through the lens of information geometry. We calculate the sensitivity of model behavior to variations in parameters. In most cases, models are sloppy, that is, exhibit an exponential hierarchy of parameter sensitivities. We propose a parameter classification scheme based on how the sensitivities scale at long observation times. We show that for oscillatory models, either with a limit cycle or a strange attractor, sensitivities can become arbitrarily large, which implies a high effective-dimensionality on the model manifold. Sloppy models with a single fixed point have model manifolds with low effective-dimensionality, previously described as a “hyper-ribbon”. In contrast, models with high effective dimensionality translate into multimodal fitting problems. We define a measure of curvature on the model manifold which we call the *winding frequency* that estimates the linear density of local minima in the model’s parameter space. We then show how alternative choices of fitting metrics can “unwind” the model manifold and give low winding frequencies. This prescription translates the model manifold from one of high effective-dimensionality into the “hyper-ribbon” structures observed elsewhere. This translation opens the door for applications of sloppy model analysis and model reduction methods developed for models with low effective-dimensionality.

An essential part of the modeling process is selecting a similarity metric that quantifies the extent to which a model mimics the system or phenomenon of interest [1]. The choice of similarity metric informs nearly all aspects of the modeling process: model selection, data fitting, model reduction, experimental design, model validation, etc.. Here, we consider the question of similarity metrics for dynamical systems, particularly oscillatory ones. Although a common choice, the nonlinear least squares metric comparing model outputs at selected times leads to models with a *high effective dimensionality*. In addition to posing technical challenges (e.g., ill-posed, multimodal fitting problems), we argue that a high effective dimensionality reflects a more fundamental issue: that the choice of metric does not accurately capture the essential properties of the system. In this paper, we use sloppy model analysis and information geometry to identify parameter combinations in models of dynamical systems that lead to high effective dimensionalities. We then use methods of signal processing to construct new similarity measures that “unwind” the model manifold and lead to well-posed inference problems.

Some have already observed that one’s choice of metric is a critical aspect of parameter space exploration [2, 3]. The relationship between model behavior and parameters is (locally) captured by sensitivity analysis. Previous studies have decomposed the sensitivities of periodic signals into independent parts that control amplitude, period, and other features [4–6]. In chaotic systems, it has been found that the dynamics exhibit an exponential sensitivity to parameters [7, 8]. In such cases, it is common to use measures of the statistical distribution

in phase space, rather than time series [3, 7, 9–11]. The present work combines these insights with tools of sloppy model analysis and information geometry.

Sloppy models are a broad class of models whose behavior exhibits an exponential hierarchy of parameter sensitivities [12–20]. Using an information geometric approach, it has been shown that the local sensitivity analysis reflects a global property, i.e., a low effective dimensionality described as a *hyper-ribbon* [21–24]. It has been suggested that this hyper-ribbon structure is why simple effective (i.e., low-dimensional) theories of collective behaviors exist for systems that are microscopically complicated [23, 24].

The effective dimensionality of sloppy models has important statistical implications. Information Criteria (such as Akaike or Bayes) are used in model selection and penalize those with too much fitting flexibility. A model’s fitting power is most easily estimated in the asymptotic limit, in which it is simply approximated by the number of parameters, i.e., the dimension of the model manifold. For hyper-ribbons, these formula greatly overestimate fitting power of a model [25, 26]. However, it is also possible for models to exhibit a *large effective dimensionality*, i.e., have model manifolds whose fitting power is much larger than that suggested by the number of parameters. As we show, these models will exhibit extreme multimodality when fit to data, and have model manifolds with large curvatures that tend to fill large volumes of behavior space.

The challenge of multimodality in fitting problems has been noted in many fields [9, 10, 27–29]. Proposals for addressing multimodality have included global search methods [9, 28, 30–32], increasing the size of the parameter space in order to escape local minima [29, 33], and changing the parameter landscape through an alternative choice of metric [3, 9].

* mktranstrum@byu.edu

In this study, we use model sensitivity analysis at long times to classify parameter combinations. In turn, we classify models based on which parameter types they include. We show that some classes of models exhibit an anomalous statistical dimension, that is, the effective dimensionality of the model may be either much more or less than the number of parameters, and argue for a deeper theoretical implication of this phenomenon. Using an information geometric approach, we relate the effective statistical dimension to the curvature on the model manifold and explicitly demonstrate that alternative metrics can lead to different effective dimensions. We present a prescription for how models of high effective dimension can be regularized through an appropriate choice of metric.

To formalize this problem, consider a parametrized model of time $y(t, \theta)$ (which could be generated, for example, as the solution to a system of differential equations), where θ is a vector of parameters and y could be either a scalar or vector of observations. We wish to quantify the similarity of the model behavior for different values of θ . The most common metric in the literature is least squares regression, in which case the distance (or cost) between two models, with parameters θ and θ_0 , takes the form

$$C(\theta) = \frac{1}{2T} \int_0^T dt [y(t, \theta) - y(t, \theta_0)]^2. \quad (1)$$

We are interested in the sensitivity of model predictions at different time scales. By increasing the total time T , this cost function defines a coarse-graining in the effective sampling rate followed by a renormalization so that the total number of effective data points is constant. When measuring the distance to observed data, the integral becomes a sum. The sensitivity of the model to infinitesimal changes in the parameters is given by the Hessian matrix evaluated at θ_0 :

$$H_{\mu\nu} = \frac{\partial^2 C}{\partial \theta_\mu \partial \theta_\nu} = \frac{1}{T} \int_0^T dt \frac{\partial y}{\partial \theta_\mu} \frac{\partial y}{\partial \theta_\nu}. \quad (2)$$

The Hessian acts as a Riemannian metric on a *model manifold* (see Refs. [21, 22]) and is the Fisher Information Metric for this measurement process. We are interested in the eigenvalues of H and their dependence on T .

In Fig. 1, we consider a cross section of the cost surface, the eigenvalues of the Hessian, and a three-dimensional projection of the model manifold for three models [34]. The first model is characterized by a transient decay to a steady state. For large T , the model becomes increasingly insensitive to parameter combinations that control transient behavior, scaling as $O(T^{-1})$. The parameter that determines the steady state scales as $O(1)$. The second model exhibits a periodic limit cycle. Parameter combinations controlling features of the attractor scale as $O(1)$, those that control the transient approach to the attractor scale as $O(T^{-1})$, and the combination controlling frequency scales as $O(T^2)$. The third model is chaotic;

parameters controlling its dynamics exhibit exponential sensitivities.

The different scaling behaviors for the Hessian eigenvalues are accompanied by different structures in both the cost surface and the model manifold. The cost surface of the first model is characterized by a single, highly anisotropic basin. Its model manifold is similarly anisotropic; the long, narrow *hyper-ribbon* structure is common for models with low effective dimensionality [21, 22]. In contrast, the second cost surface has many local minima and a model manifold with high curvature. The third cost surface exhibits a fractal-like roughness (although for finite T the derivative with respect to parameters formally exists everywhere). Its model manifold is even more highly curved and space-filling.

These three models are prototypes of three model classes, distinguished by the scaling behavior of the largest eigenvalue for large T . For the first class, $\lambda_{max} \sim O(1)$ is bound by a constant. For the second class, $\lambda_{max} \sim O(T^n)$ is bound by a polynomial. For the third class, $\lambda_{max} \sim O(e^T)$ is exponential. We plot the eigenvalue spectra of additional models from each class (at large, fixed T) in Fig. 2 [35]. Because these models all exhibit sloppy eigenvalue spectra, we refer to these model classes as *sloppy models of the first, second, and third kinds*, respectively.

The large sensitivities of sloppy models of the second and third kinds are necessarily associated with large curvature on the model manifold. This can be understood by noting that the absolute variation in the model behavior is bounded (the models oscillate, rather than grow). Large parameter sensitivities imply that the model manifold has arbitrarily large proper volume that is compressed into a bounded region of embedding space at large T by tightly winding or folding the manifold. Such manifolds effectively fill higher dimensional volumes leading to high effective dimensionality; this is the opposite effect of the arguments for low effective dimensionality in previous studies of sloppy models [23, 24].

To quantify this effect, the extrinsic curvature associated with parameter direction v is given by the geodesic curvature $k(v) = 1/R$ (as in Ref. [22]), where R is the radius of curvature of the circle tangent to the manifold along direction $(\partial y / \partial \theta^\mu) v^\mu$. We define the *winding frequency*,

$$\omega(v) \equiv \left| \frac{\partial y}{\partial \theta^\mu} v^\mu \right| k(v), \quad (3)$$

which has the interpretation of being the angular frequency at which the manifold winds around the tangent circle, such that $f = \omega/2\pi$ is both the number of windings of the manifold per unit change in parameters and the frequency of local minima in the cost as we move along direction v .

Figure 3 shows winding frequencies along Hessian eigendirections for the models from Fig. 2. Notice that sloppy models of the first kind (i.e., hyper-ribbons) have low winding frequencies. Sloppy models of the second

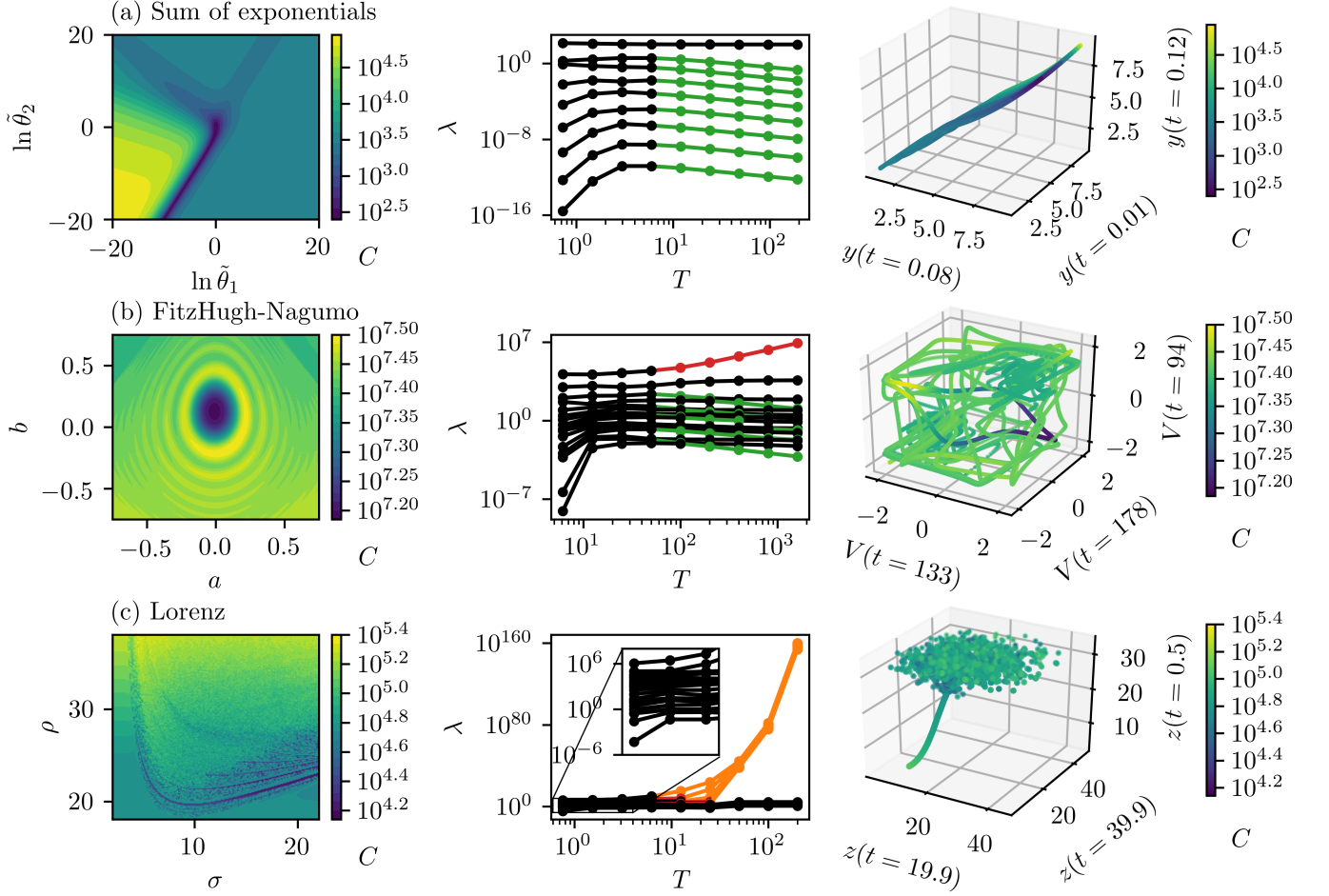


FIG. 1. **Model classes.** 1^{st} column: Cost cross sections for three prototype models. Contrast the canyons in (a) with the ripples in (b) and the roughness in (c). 2^{nd} column: Hessian eigenvalues as a function of sampling time. Colors differentiate scaling behaviors at long times. 3^{rd} column: Projections of the model manifold. In (a), a 3-ball in parameter space is mapped to a nearly 1-dimensional region of prediction space. By contrast, for (b) and (c) a single parameter is varied producing a 1D (space-filling) curve in prediction space. In (c), the model goes through a bifurcation where the manifold begins to oscillate rapidly. The sampling required to see continuity is prohibitive, so the points plotted become scattered.

kind have high winding frequency in the stiffest direction which controls frequency. Sloppy models of the third kind have high winding frequencies in most or all directions.

The effective dimensionality, estimated by the winding frequencies, depends on the metric of the model manifold embedding space, i.e., Eq. (1). We now show that alternative choices for embedding the model manifold can lead to different effective dimensionalities.

The high effective dimensionality of sloppy models of the second kind is due entirely to the parameter combination controlling frequency. Varying this parameter combination causes model predictions to pass in and out of phase with each other, resulting in local minima in the cost. We avoid this aliasing by defining the phase of oscillation as a monotonically increasing function of time. Many definitions of instantaneous frequency and phase have been considered in the literature [36, 37]. We use the *analytic signal* approach [38], which defines the

phase $\phi(t)$ of an oscillation $y(t)$ by the relation

$$z(t) = y(t) + iH[y](t) = A(t)e^{i\phi(t)}, \quad (4)$$

where $z(t)$ is the analytic signal whose complex argument is the phase of oscillation, and $H[y](t)$ is the Hilbert transform of $y(t)$ [39]. We define a new signal \tilde{y} as a function of phase:

$$\tilde{y}(\phi, \theta) \equiv y(t(\phi), \theta), \quad (5)$$

and construct a cost by comparing models at the same phase rather than time. Importantly, note that ϕ depends on parameters. To account for this, we expand \tilde{y} to lowest order in ϕ , in which case the cost becomes

$$C(\theta) \equiv \frac{1}{2T} \int_0^{\phi(T, \theta_0)} d\phi (\delta\tilde{y} + \frac{\partial\tilde{y}}{\partial\phi} \delta\phi)^2, \quad (6)$$

$$\delta\tilde{y} \equiv \tilde{y}(\phi(\theta_0), \theta) - \tilde{y}(\phi(\theta_0), \theta_0), \quad (6a)$$

$$\delta\phi \equiv \phi(\theta) - \phi(\theta_0). \quad (6b)$$

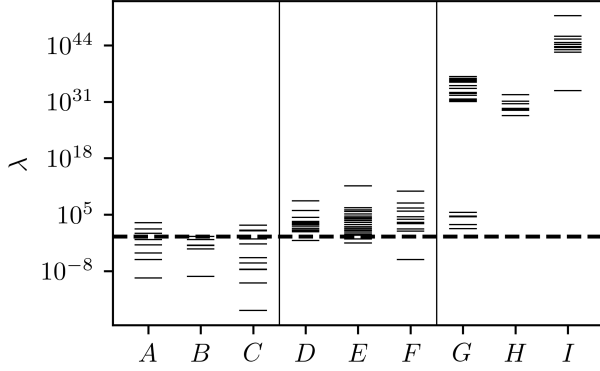


FIG. 2. **Eigenvalues of the FIM** for the following models: A) sum of exponentials; B) rational polynomial; C) biological adaptation; D) FitzHugh-Nagumo; E) Hodgkin-Huxley; F) Wnt oscillator; G) Lorenz; H) Hindmarsh-Rose; I) damped, driven pendulum. A, B, C are nonoscillatory models, D, E, F are periodic, and G, H, I are chaotic.

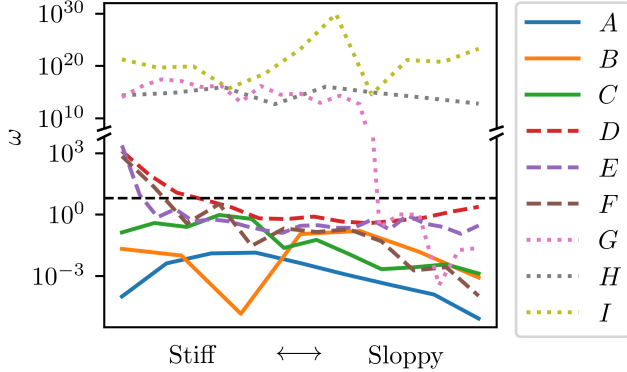


FIG. 3. **Winding frequencies** along Hessian eigendirections for the models from Fig. 2. The black dashed line at $\omega = 2\pi$ roughly distinguishes low from high winding frequencies.

This definition is a quadratic approximation of Eq. (1) that preserves the Hessian in Eq. (2), i.e., it is an isometric embedding of the model manifold [40]. However, because changes in frequency only affect $\phi(\theta)$, which is unbounded, the large manifold volume is not constrained to a finite region of the embedding space.

We implement the new metric for the FitzHugh-Nagumo model as an example; results are shown in Fig. 4(a). The ripples in the cost surface in Fig. 1(b) are replaced by a smooth basin, the winding frequency of the stiffest direction is significantly reduced, and the manifold is no longer highly curved. Because the new cost function is an isometric embedding [i.e., preserves the Hessian in Eq. (2)], the curvature of the cost surface at the bottom of the bowl is the same as that in Fig. 1(b).

The high effective dimensionality of sloppy models of the third kind cannot be eliminated using analytic signal. The exponential sensitivities of chaotic systems make

time series prediction impossible at long times. However, model predictions $y_i(\theta)$ do give rise to a predictable density $f(y, \theta)$ in phase space [11]. We evolve an ensemble of initial conditions and use the result to approximate this density with a *kernel density estimate* [41, 42],

$$f(y, \theta) \approx \frac{1}{nh} \sum_{i=1}^n K\left(\frac{y - y_i(\theta)}{h}\right), \quad (7)$$

where n is the number of predictions/observations, K is a kernel function, and h is the kernel bandwidth. A natural metric to use for distributions is the *Hellinger distance*:

$$C(\theta) \equiv \frac{1}{2} \int dy \left(\sqrt{f(y, \theta)} - \sqrt{f(y, \theta_0)} \right)^2. \quad (8)$$

We implement this cost for the Lorenz system; results are shown in Fig. 4(b). The rough cost surface of Fig. 1(c) has been replaced with another basin, the high winding frequencies have all disappeared, and the manifold is now regular.

Multimodality in comparing and training multi-parameter models is a common problem [9, 10, 27–29]. Here, we have shown how the choice of distance measure affects the number of local minima. We have quantified this effect using curvature on the model manifold and introduced the *winding frequency* to estimate the density of local minima in parameter space. Finally, we have shown that through an appropriate choice of metric, the model manifold can be systematically “unwound” to remove local minima while preserving relevant physical interpretations of distance.

One of the ongoing challenges for many complex systems is the development of appropriate reduced-order representations [23, 43–45]. More broadly, it has been suggested that the existence of useful simplified models is often due to a systematic compression of parameter space [23]. Compressing the parameter space leads to a type of “universality class” in which models with different parameter values make statistically indistinguishable predictions. This line of work has also led to new methods for constructing simplified models from more complex and complete mechanistic representations [46]. Ultimately, this compression is a consequence of the similarity metric used to compare model behaviors.

For sloppy models of the first kind (which have previously dominated the literature), the compression “squashes” some dimensions to be very thin (as in Fig. 1(a) and Refs. [21, 22]), leading to a universality class of continuously-connected parameters for which reduced-order models can be systematically derived [46]. In contrast, for sloppy models of the second and third kind, the manifold is wound tightly, so that a compression leads to a manifold folding in which non-contiguous regions of the manifold are identified as part of the same universality class. It is unlikely that predictive reduced-order models can be found for sloppy models with high winding numbers as this would imply the existence, for example, of accurate long-term weather forecasts. Large winding

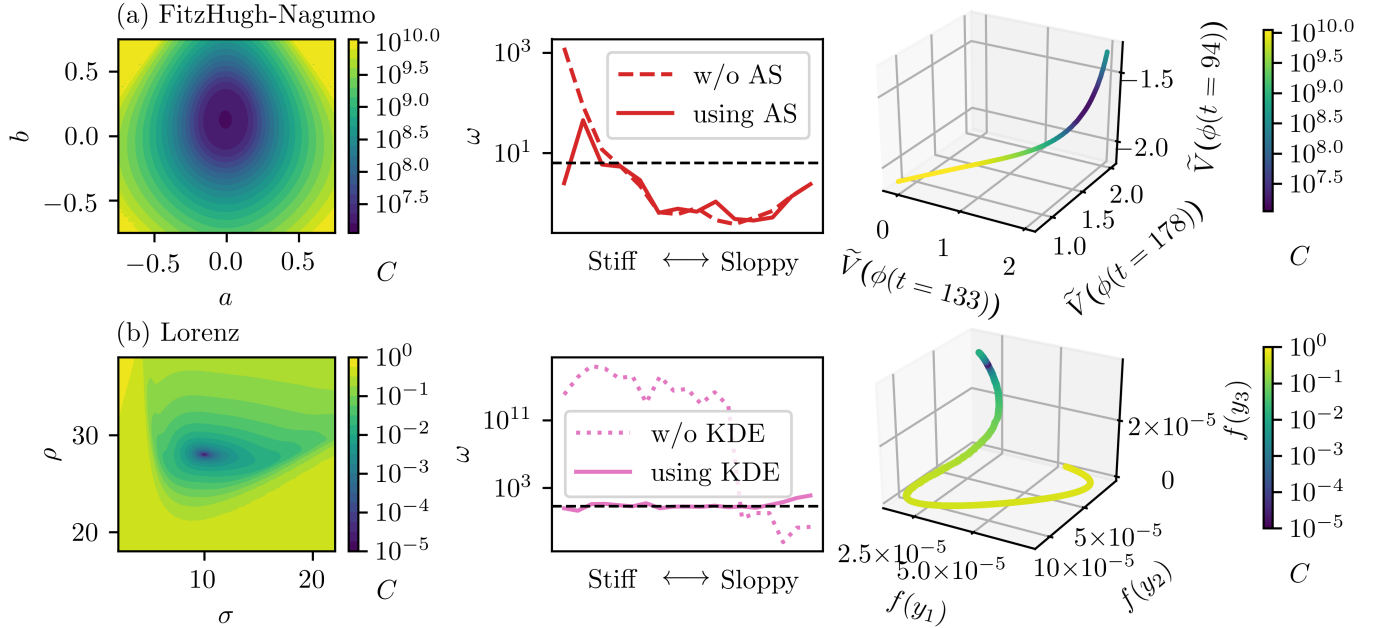


FIG. 4. **Effects of alternative metrics**, (a) using analytic signal (AS) and (b) using kernel density estimation (KDE). 1^{st} column: Cost cross sections. 2^{nd} column: Winding frequencies. 3^{rd} column: Manifold projections.

number is the information-geometric equivalent of sensitivity to microscopic details, well-studied in chaotic systems. In contrast, by unwinding the model manifold using an alternative metric, the manifold is transformed into a hyper-ribbon and this extreme-sensitivity to microscopic details is removed.

Understanding how effective theories emerge at long time scales is a challenging problem that has drawn on sophisticated expertise from a variety of fields, including dynamical systems [47, 48], signal processing [4, 6], statistics [26, 49], and optimization [10, 29]. In this work we have combined insights from these other domains with tools of information geometry. Our hope is that this ex-

plicit connection will bring new tools, such as sloppy model analysis and the manifold boundary approximation method, to bear on a wide range of important, ongoing scientific problems.

ACKNOWLEDGMENTS

We thank Alex Stankovic for helpful comments. Resources at the Fulton Supercomputing Lab at Brigham Young University were used for many of the computations. BLF and MKT were supported by the National Science Foundation through grant NSF EPCN-1710727.

-
- [1] (): Although our interest here is in mathematical models, the same is true of model organisms in biology that, by virtue of being (for example) mammals, vertebrates, eukaryotes, etc., have a similar phylogeny to a target system, e.g., humans.
 - [2] M. Pospischil, M. Toledo-Rodriguez, C. Monier, Z. Pivkowska, T. Bal, Y. Frégnac, H. Markram, A. Destexhe: *Biological cybernetics* **99** (2008) 427
 - [3] G. LeMasson, R. Maex: In: *Computational Neuroscience: Realistic Modeling for Experimentalists*, ed. E. De Schutter, chap. 1 pp. 1–24. CRC Press (2000)
 - [4] M. A. Kramer, H. Rabitz, J. M. Calo: *Applied mathematical modelling* **8** (1984) 328
 - [5] R. Larter, H. Rabitz, M. Kramer: *The Journal of chemical physics* **80** (1984) 4120
 - [6] A. K. Wilkins, B. Tidor, J. White, P. I. Barton: *SIAM Journal on Scientific Computing* **31** (2009) 2706
 - [7] D. J. Lea, M. R. Allen, T. W. Haine: *Tellus A: Dynamic Meteorology and Oceanography* **52** (2000) 523
 - [8] V. Pisarenko, D. Sornette: *Physical Review E* **69** (2004) 036122
 - [9] J. Annan, J. Hargreaves: *Tellus A* **56** (2004) 520
 - [10] A. C. Lorenc, T. Payne: *Quarterly Journal of the Royal Meteorological Society* **133** (2007) 607
 - [11] A. Lasota, M. C. Mackey: *Chaos, fractals, and noise: stochastic aspects of dynamics*, vol. 97: Springer Science & Business Media (2013)
 - [12] K. S. Brown, J. P. Sethna: *Physical Review E* **68** (2003) 021904
 - [13] K. S. Brown, C. C. Hill, G. A. Calero, C. R. Myers, K. H. Lee, J. P. Sethna, R. A. Cerione: *Physical biology* **1** (2004) 184
 - [14] S. L. Frederiksen, K. W. Jacobsen, K. S. Brown, J. P. Sethna: *Physical review letters* **93** (2004) 165501

- [15] J. J. Waterfall, F. P. Casey, R. N. Gutenkunst, K. S. Brown, C. R. Myers, P. W. Brouwer, V. Elser, J. P. Sethna: *Physical review letters* **97** (2006) 150601
- [16] R. Gutenkunst: *Sloppiness, modeling, and evolution in biochemical networks*: Ph.D. thesis, Cornell University (2007)
- [17] F. P. Casey, D. Baird, Q. Feng, R. N. Gutenkunst, J. J. Waterfall, C. R. Myers, K. S. Brown, R. A. Cerione, J. P. Sethna: *IET systems biology* **1** (2007) 190
- [18] R. N. Gutenkunst, F. P. Casey, J. J. Waterfall, C. R. Myers, J. P. Sethna: *Annals of the New York Academy of Sciences* **1115** (2007) 203
- [19] R. N. Gutenkunst, J. J. Waterfall, F. P. Casey, K. S. Brown, C. R. Myers, J. P. Sethna: *PLoS computational biology* **3** (2007) e189
- [20] B. C. Daniels, Y.-J. Chen, J. P. Sethna, R. N. Gutenkunst, C. R. Myers: *Current opinion in biotechnology* **19** (2008) 389
- [21] M. K. Transtrum, B. B. Machta, J. P. Sethna: *Physical review letters* **104** (2010) 060201
- [22] M. K. Transtrum, B. B. Machta, J. P. Sethna: *Physical Review E* **83** (2011) 036701
- [23] B. B. Machta, R. Chachra, M. K. Transtrum, J. P. Sethna: *Science* **342** (2013) 604
- [24] M. K. Transtrum, B. B. Machta, K. S. Brown, B. C. Daniels, C. R. Myers, J. P. Sethna: *The Journal of chemical physics* **143** (2015) 07B201.1
- [25] C. H. LaMont, P. A. Wiggins: *stat* **1050** (2016) 24
- [26] C. H. LaMont, P. A. Wiggins: *arXiv preprint arXiv:1506.05855v4* (2017)
- [27] P. Mendes, D. Kell: *Bioinformatics (Oxford, England)* **14** (1998) 869
- [28] C. G. Moles, P. Mendes, J. R. Banga: *Genome research* **13** (2003) 2467
- [29] J. O. Ramsay, G. Hooker, D. Campbell, J. Cao: *Journal of the Royal Statistical Society: Series B (Statistical Methodology)* **69** (2007) 741
- [30] L. Yao, W. A. Sethares: *IEEE Transactions on signal processing* **42** (1994) 927
- [31] Q. He, L. Wang, B. Liu: *Chaos, Solitons & Fractals* **34** (2007) 654
- [32] M. Rodriguez-Fernandez, P. Mendes, J. R. Banga: *Biosystems* **83** (2006) 248
- [33] E. Baake, M. Baake, H. Bock, K. Briggs: *Physical Review A* **45** (1992) 5524
- [34] (): See Supplemental Material for mathematical details.
- [35] (): See Supplemental Material for mathematical details.
- [36] B. Boashash: *Proceedings of the IEEE* **80** (1992) 520
- [37] A. S. Pikovsky, M. G. Rosenblum, G. V. Osipov, J. Kurths: *Physica D: Nonlinear Phenomena* **104** (1997) 219
- [38] D. Gabor: *Electrical Engineers-Part III: Radio and Communication Engineering, Journal of the Institution of* **93** (1946) 429
- [39] (): See Supplemental Material for mathematical details.
- [40] (): See Supplemental Material for a proof.
- [41] M. Rosenblatt: *The Annals of Mathematical Statistics* (1956) 832
- [42] E. Parzen: *The annals of mathematical statistics* **33** (1962) 1065
- [43] P. W. Anderson, et al.: *Science* **177** (1972) 393
- [44] C. Theodoropoulos, Y.-H. Qian, I. G. Kevrekidis: *Proceedings of the National Academy of Sciences* **97** (2000) 9840
- [45] M. K. Transtrum, P. Qiu: *PLoS computational biology* **12** (2016) e1004915
- [46] M. K. Transtrum, P. Qiu: *Physical review letters* **113** (2014) 098701
- [47] C. W. Gear, J. M. Hyman, P. G. Kevrekidis, I. G. Kevrekidis, O. Runborg, C. Theodoropoulos: *Communications in Mathematical Sciences* **1** (2003) 715
- [48] M. Desroches, J. Guckenheimer, B. Krauskopf, C. Kuehn, H. M. Osinga, M. Wechselberger: *Siam Review* **54** (2012) 211
- [49] H. H. Mattingly, M. K. Transtrum, M. C. Abbott, B. B. Machta: *Proceedings of the National Academy of Sciences* **115** (2018) 1760
- [50] R. Chachra, M. K. Transtrum, J. P. Sethna: *Physical Review E* **86** (2012) 026712
- [51] W. Ma, A. Trusina, H. El-Samad, W. A. Lim, C. Tang: *Cell* **138** (2009) 760
- [52] R. FitzHugh: *Biophysical journal* **1** (1961) 445
- [53] J. Nagumo, S. Arimoto, S. Yoshizawa: *Proceedings of the IRE* **50** (1962) 2061
- [54] A. L. Hodgkin, A. F. Huxley: *The Journal of physiology* **117** (1952) 500
- [55] P. B. Jensen, L. Pedersen, S. Krishna, M. H. Jensen: *Biophysical journal* **98** (2010) 943
- [56] E. N. Lorenz: *Journal of the atmospheric sciences* **20** (1963) 130
- [57] J. Hindmarsh, R. Rose: *Proceedings of the Royal Society of London B: Biological Sciences* **221** (1984) 87
- [58] X.-J. Wang: *Physica D: Nonlinear Phenomena* **62** (1993) 263
- [59] I. Z. Kiss, J. L. Hudson: *Physical Review E* **64** (2001) 046215
- [60] N. E. Huang, Z. Shen, S. R. Long, M. C. Wu, H. H. Shih, Q. Zheng, N.-C. Yen, C. C. Tung, H. H. Liu: *Proceedings of the Royal Society of London A: Mathematical, Physical and Engineering Sciences* **454** (1998) 903
- [61] T. Yalçinkaya, Y.-C. Lai: *Physical Review Letters* **79** (1997) 3885

Supplemental Material

Appendix A: Models

Following are the models examined in Figs. 1, 2, 3, and 4. In some cases, additional polynomial terms (with parameters as coefficients) were added to the model equations of motion. This allows calculation of the *structural susceptibility* of the model, that is, susceptibility to perturbations of the underlying dynamics [50]. These terms can be thought of as representing details of the real system that have been left out of the model.

A) A sum of decaying exponentials leading to a steady state:

$$y(t; \theta) = \theta_1 + \sum_{n=2}^N e^{-\sum_{i=2}^n \theta_i t} \quad (\text{A1})$$

B) A rational polynomial model:

$$y(t; \theta) = \frac{\theta_1 + \theta_2 t + \theta_3 t^2 + \theta_4 t^3}{1 + \theta_5 t + \theta_6 t^2 + \theta_7 t^3} \quad (\text{A2})$$

C) We use the IFFLP model of biological adaptation described in [51].

D) The FitzHugh-Nagumo model [29, 52, 53] can be written as:

$$\dot{V} = c \left(V - \frac{V^3}{3} + R \right) \quad (\text{A3a})$$

$$\dot{R} = -\frac{1}{c}(V - a + bR) \quad (\text{A3b})$$

E) We implement the Hodgkin-Huxley model described in [54].

F) We use the Wnt oscillator model described in [55].

G) The Lorenz system [56] is given by:

$$\dot{x} = \sigma(y - x) \quad (\text{A4a})$$

$$\dot{y} = x(\rho - z) - y \quad (\text{A4b})$$

$$\dot{z} = xy - \beta z \quad (\text{A4c})$$

Additional parameters for rescaling x , y , and z (after solving the ODE) were also included. These would account for differences in units between the model and the observations.

H) The Hindmarsh-Rose model [57, 58] can be written as:

$$\dot{x} = y - ax^3 + bx^2 - z + I \quad (\text{A5a})$$

$$\dot{y} = c - dx^2 - y \quad (\text{A5b})$$

$$\dot{z} = \epsilon \left(x - \frac{1}{s}(z - z_R) \right) \quad (\text{A5c})$$

I) The equations of motion for a damped, driven pendulum (derivable using Newton's 2nd law) are:

$$\dot{\theta} = \omega \quad (\text{A6a})$$

$$\dot{\omega} = -\frac{\omega}{Q} - \sin(\theta) + A \cos(\phi) \quad (\text{A6b})$$

$$\dot{\phi} = \omega_D. \quad (\text{A6c})$$

1. Convergence of costs and manifolds

In Fig. 4, a sufficiently large number of time points was included in the cost and manifold calculations to demonstrate the results of using the new metrics in the limit of infinite time. In practice, only a finite number of time points can be included. Here we demonstrate the convergence of the FitzHugh-Nagumo manifold and the Lorenz cost as a function of the number of sampled time points.

Figure 5 shows two projections of the FitzHugh-Nagumo manifold (signal predictions at constant phase): one calculated using about 24 time points per cycle in the original time series and the other using twice the time sampling of the first. The manifold itself exhibits oscillations in both cases. These oscillations are an artifact of the finite time sampling of the oscillatory signal predicted by the model. As parameters that control frequency are varied, the peak of each cycle shifts between adjacent time points and the local amplitude appears to oscillate (see Fig. 6). Hence the predicted signal values at a given (constant) phase also oscillate, resulting in the manifold oscillations observed.

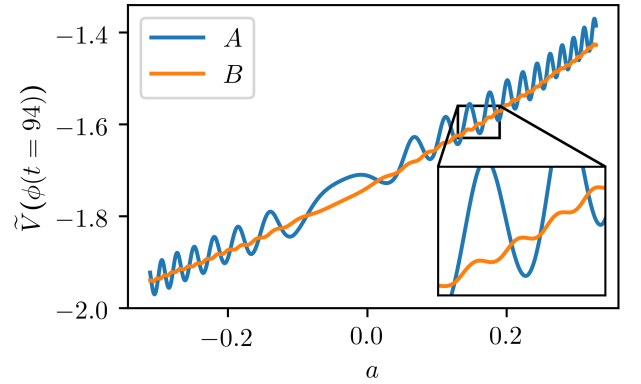


FIG. 5. **FitzHugh-Nagumo manifold projection.** A was calculated using about 24 time points per cycle in the original time series; B was calculated using twice the time sampling of A .

As demonstrated in Fig. 5, doubling the sampling of time points doubles the frequency of these manifold oscillations, but their amplitude decreases by a factor of ~ 10 . Hence, in the limit of infinite sampling they disappear. In practice they will be negligible as long as enough time

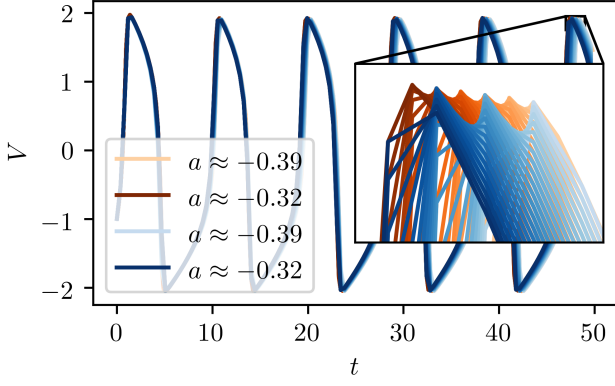


FIG. 6. **FitzHugh-Nagumo amplitude oscillations.** Colors are the same as in Fig. 5. As the peak moves between sampled time points, the amplitude appears to oscillate.

points per cycle are sampled for the amplitude of the oscillations to be small compared to the amplitude of the signal itself (and to changes effected by the parameters).

The attractors of chaotic systems have fractal structure that is realized only in the limit of infinite sampling time T . Accordingly, as more time points are included, the kernel density estimate Eq. (7) will approach the true distribution $f(y, \theta)$ asymptotically. Figure 7 illustrates the convergence of a cross section of the cost Eq. (8) for the Lorenz system as the total sampling time T is varied.

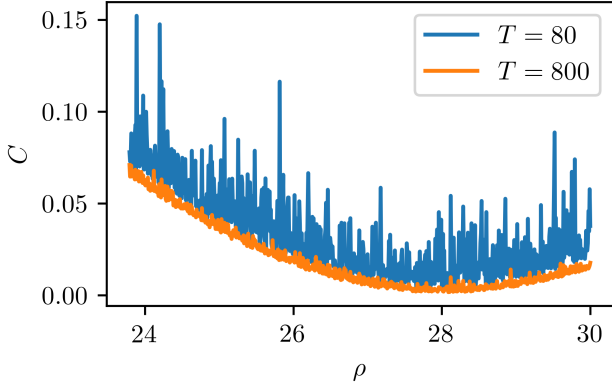


FIG. 7. **Lorenz cost.** As the number of sampled time points grows, the noise in the cost dies away. The MAEs between a parabolic fit and each of the two cost estimates are 0.0088 for $T = 80$ and 0.0013 for $T = 800$ (about a sevenfold reduction in noise).

Appendix B: Sensitivity analysis

Here we describe the sensitivity analysis leading to the scaling behavior of the eigenvalues of the Hessian described in the main text.

Models in the first class (nonoscillatory) exhibit tran-

sient dynamics leading to a steady state. Parameter combinations that control the transient dynamics must have sensitivities that decay to zero at long times,

$$\frac{\partial y}{\partial \theta_\mu}(t \rightarrow \infty) \sim 0, \quad (\text{B1})$$

while those that control the steady state are asymptotically constant:

$$\frac{\partial y}{\partial \theta_\mu}(t \rightarrow \infty) \sim \text{const.} \quad (\text{B2})$$

Given Eq. (2), this leads to the $O(T^{-1})$ and $O(1)$ scaling behaviors of these two parameter types. This can be understood in the following way: recall that the Hessian is the Fisher Information Metric (FIM) for this measurement process. As the total sampling time T is increased past the transient dynamics, the only additional information gained is information about the final steady state. Normalizing by T amounts to increasing the sampling time while decreasing the sampling rate, so we lose information about the transient dynamics but not about the steady state by going to long times.

In periodic oscillatory models, there may also be transient dynamics leading to a (now cyclic) steady state, hence the $O(T^{-1})$ and $O(1)$ scaling behaviors can still occur. However, the dynamics have the additional feature of having a frequency of oscillation. Parameters controlling the frequency have a distinct scaling behavior, which can be seen as follows. The steady state predicted by the model may be expanded in a Fourier series:

$$y(t; \theta) = \sum_{k=-\infty}^{\infty} c_k(\theta) e^{ik\omega(\theta)t} \quad (\text{B3})$$

$$= y(t; c(\theta), \omega(\theta)) \quad (\text{B4})$$

This decomposes the parameter sensitivities into two parts:

$$\frac{\partial y}{\partial \theta_\mu} = \sum_{k=-\infty}^{\infty} \frac{\partial y}{\partial c_k} \frac{\partial c_k}{\partial \theta_\mu} + \frac{\partial y}{\partial \omega} \frac{\partial \omega}{\partial \theta_\mu} \quad (\text{B5})$$

Because c_k and ω are time-independent by construction, the time dependence is due entirely to the coefficients

$$\frac{\partial y}{\partial c_k} = e^{ik\omega(\theta)t}, \quad (\text{B6})$$

which is bounded by a constant, and

$$\frac{\partial y}{\partial \omega} = \sum_{k=-\infty}^{\infty} ikt c_k(\theta) e^{ik\omega(\theta)t} \propto t, \quad (\text{B7})$$

which grows linearly with time. The amplitude sensitivities $(\partial y / \partial c_k)(\partial c_k / \partial \theta_\mu)$ control the shape and amplitude of the steady state and give rise to $O(1)$ scaling behavior. By contrast, the frequency sensitivity $(\partial y / \partial \omega)(\partial \omega / \partial \theta_\mu)$

(note that there is exactly one) results in $O(T^2)$ scaling behavior (refer again to Eq. (2)). Other studies have focused on the sensitivity to period, rather than frequency, but the scaling behavior is the same for both [4–6].

Finally, in chaotic models, all of the parameter sensitivities affecting the dynamics exhibit exponential growth at long times:

$$\frac{\partial y}{\partial \theta_\mu}(t \rightarrow \infty) \sim e^{\lambda_\mu t}, \quad (\text{B8})$$

so we expect all eigenvalues to go as $O(e^T)$.

These observations lead us to a classification of the parameters of a model, in addition to the classification of the model itself (see Table I). LaMont and Wiggins have also proposed a classification of model parameters, based on the *complexity* of a given parameter combination [25]. In the case of dynamical models, our analysis illustrates the mechanisms that give rise to the complexities of each class.

TABLE I. Parameter classification

Eigenvalue behavior	Parameter controls
$O(T^{-1})$	transient dynamics
$O(1)$	steady state
$O(T^2)$	frequency
$O(e^T)$	chaotic dynamics

Appendix C: Analytic signal

Calibrating mathematical models typically involves matching a set of model predictions, e. g., $y(t_i, \theta)$, at times t_i , for some parameters θ to experimental observations y_i , occasionally with uncertainties σ_i . The predictions that give the best fit to the data are those that minimize the cost function C , defined as a weighted sum of squares:

$$C(\theta) = \frac{1}{2} \sum_i \left(\frac{y(t_i, \theta) - y_i}{\sigma_i} \right)^2. \quad (\text{C1})$$

This may be generalized for cases where a full covariance matrix Σ is given, rather than individual uncertainties σ_i . Defining the deviations $\delta y_i \equiv y(t_i, \theta) - y_i$ and the deviation vector $\delta y \equiv (\delta y_1, \delta y_2, \dots, \delta y_M)$, with M the number of observations, the cost is

$$C(\theta) = \frac{1}{2} \delta y^T \Sigma^{-1} \delta y. \quad (\text{C2})$$

Such a cost compares observations and predictions at the same time. The Fisher Information Matrix (FIM) for this cost is

$$I = \frac{\partial y^T}{\partial \theta} \Sigma^{-1} \frac{\partial y}{\partial \theta} \quad (\text{C3})$$

and is a measure of the amount of information that can be obtained about the parameters from the observations.

When the model is linear in the parameters, the cost is quadratic and the best fit can be expressed analytically. However, in the case of oscillatory systems, parameters that affect frequency are necessarily nonlinear and result in local minima in the cost function (see Fig. 8). Figure 9, upper left panel, shows two oscillations with mismatched amplitudes and frequencies and their difference. The difference in frequency is penalized appropriately when the oscillations are out of phase but not when they are in phase at later times. The local minima resulting from this aliasing can be avoided by comparing observations to predictions at the same phase of oscillation (upper left panel), rather than at the same time.

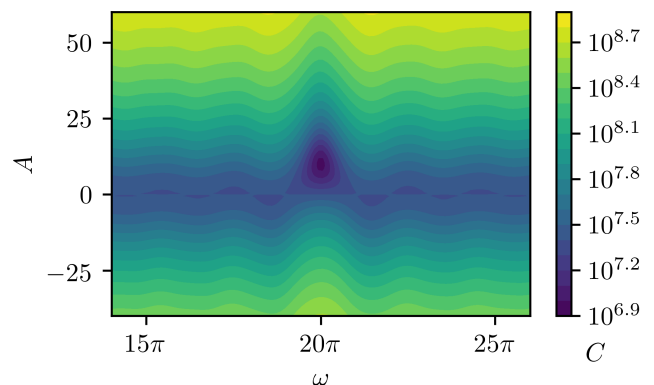


FIG. 8. **Least squares cost** for the model $y(t) = A \cos(\omega t)$, treating A and ω as parameters. Local minima are apparent.

The idea of calculating the phase of an oscillatory system is not new. Boashash reviews the historical development of definitions of instantaneous frequency, and Pikovsky, et. al. present several possible definitions of phase for a chaotic system [36, 37]. We discuss one of these as our primary method of obtaining a phase in Sec. C1. An alternative is discussed in Sec. C6 as a way to avoid numerical issues which we also discuss in that section. The first method was used by Kiss and Hudson to calculate the instantaneous phase of a particular chaotic oscillator as an intermediate step in defining phase synchronization [59]. However, to the authors' knowledge, this is the first time using phase has been proposed to change the shape of the cost for an oscillatory system.

Phases derived from observations will have uncertainty; therefore it is necessary to propagate uncertainty from the latter to the former. In addition, the uncertainty of the observations with phase as the independent variable will differ from their uncertainty as a function of time. We consider propagation of uncertainty by deriving covariance matrices 1) for the phases and 2) for the observations with phase as the independent variable in Sec. C2. Both the observations and their corresponding phases contain information that should be accounted for.

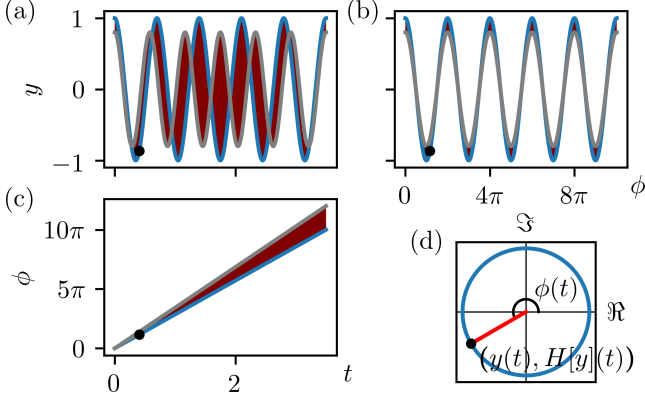


FIG. 9. **Decoupling amplitude from phase.** (a) Signal vs. time for two signals with mismatched amplitude and frequency; their difference is indicated in dark red. The mismatch in frequency results in a large penalty δy when the two signals are out of phase ($t \approx 1.8$) but little or no penalty when they are in phase ($t \approx 3.5$). (b) Signal vs. phase for the same signals. The difference in amplitude results in a consistent penalty $\delta \tilde{y}$ throughout (see Sec. C 2 b). (c) Phase vs. time for the two signals. The difference in frequency is correctly penalized in $\delta \phi$ at late times (see Sec. C 2 a). (d) Analytic representation in the complex plane of the black point marked in the other 3 panels (see Sec. C 1).

We propose a new cost for oscillatory systems that includes both sets of information in Sec. C 3. We show that the FIM is fully preserved in the new scheme in Sec. C 4. Calculation of winding frequencies requires second-order parameter sensitivities of both phase and model predictions. We give explicit formulas for these in Sec. C 5.

Because a proper phase, like time, is monotonically increasing, it can only be defined for dynamical variables that have a unique center of oscillation. For cases where there is not a unique center of oscillation, see Sec. C 6.

1. Phase definition

We motivate our definition of the phase with the following example. The signal $x(t) = A \cos(\omega t + \phi_0)$ may be interpreted as the projection onto the x -axis of motion in the xy -plane around a circle of radius A , with frequency ω . The projection onto the y -axis gives $y(t) = A \sin(\omega t + \phi_0)$. The phase of oscillation $\phi(t)$ can be almost-unambiguously defined (up to multiples of 2π) as the angle of each point $(x(t), y(t))$ with respect to the positive x -axis:

$$\begin{aligned} \phi(t) &= \tan^{-1} \left(\frac{y(t)}{x(t)} \right) \\ &= \tan^{-1} \left(\frac{A \sin(\omega t + \phi_0)}{A \cos(\omega t + \phi_0)} \right) \\ &= \tan^{-1}(\tan(\omega t + \phi_0)) \\ &= \omega t + \phi_0. \end{aligned} \quad (\text{C4})$$

By analogy with this example, we can obtain the phase of the signal $y(t)$ if we can unambiguously extend it from one dimension to two. We accomplish this using a concept from signal processing known as the *analytic signal* [38]. The analytic signal $z(t)$ is a complex function defined as

$$z(t) \equiv y(t) + iH[y](t) = A(t)e^{i\phi(t)}, \quad (\text{C5})$$

where $H[y](t)$ is the *Hilbert transform* of $y(t)$,

$$H[y](t) \equiv \frac{1}{\pi} \text{PV} \int_{-\infty}^{\infty} \frac{y(\tau)}{t - \tau} d\tau, \quad (\text{C6})$$

and the magnitude $A(t)$ and argument $\phi(t)$ are

$$A(t) \equiv \sqrt{y^2(t) + H^2[y](t)} \quad (\text{C7})$$

$$\phi(t) \equiv \tan^{-1} \left(\frac{H[y](t)}{y(t)} \right) \quad (\text{C8})$$

[see Fig. 9(d)]. We take Eq. (C8) as our definition of the phase of oscillation.

Given Eq. (C5), we may write

$$y(t) = \Re(z(t)) = A(t) \cos(\phi(t)). \quad (\text{C9})$$

This allows us to reinterpret the oscillatory signal as a function of phase:

$$\tilde{y}(\phi(t)) \equiv y(t) = A(t) \cos(\phi(t)). \quad (\text{C10})$$

Assuming $\phi(t)$ is monotonically increasing, the relationship between ϕ and t is invertible. Hence, we may also write

$$\tilde{y}(\phi) = A(t(\phi)) \cos(\phi). \quad (\text{C11})$$

This allows observations and predictions to be compared at the same phase. We will return to this point in the next section.

If the signal $y(t)$ is a vector, rather than scalar, quantity (that is, if the system has multiple dynamical variables), the preceding prescription should be applied separately to each scalar component, producing a vector of phases. Alternatively, it may be applied to a single scalar component of y , and the resulting phase may be used for all of the components.

Additionally, a necessary condition for $\phi(t)$ to be monotonically increasing is that the signal $y(t)$ oscillate around 0. If it is not, the time average $\langle y(t) \rangle = (1/T) \int_0^T y(t) dt$ should be subtracted from $y(t)$ prior to calculating the phase. Note that $H[y](t)$ will be unaffected, as the Hilbert transform of a constant is 0.

2. Covariance matrices

We now consider how uncertainty in the observations propagates to the phases derived from them. First, we

define more precisely the covariance matrix $\Sigma^{y(t)}$ for the observations with time as the independent variable. We assume the observations y_i are random variables that are normally distributed about the predictions $y(t_i, \theta_0)$ of the model at the best fit, with standard deviation given by the uncertainties σ_i :

$$y_i = y(t_i, \theta_0) + \sigma_i \xi_i. \quad (\text{C12})$$

(ξ_i are random variables drawn from the normal distribution, $N(0, 1)$.) The deviations $\delta y_i = \delta y_i(\theta)$ vary with the predictions of the model. Evaluated at the best fit they are random variables with mean 0 and standard deviation σ_i :

$$\begin{aligned} \delta y_i(\theta) &= y(t_i, \theta) - y_i \\ &= y(t_i, \theta) - y(t_i, \theta_0) - \sigma_i \xi_i \end{aligned} \quad (\text{C13})$$

$$\delta y_i(\theta_0) = -\sigma_i \xi_i. \quad (\text{C14})$$

The elements of the covariance matrix are defined as the expectation of the product of deviations at the best fit:

$$\begin{aligned} \Sigma_{ij}^{y(t)} &\equiv \langle \delta y_i \delta y_j \rangle \\ &= \langle \sigma_i \xi_i \sigma_j \xi_j \rangle \\ &= \sigma_i \sigma_j \langle \xi_i \xi_j \rangle. \end{aligned} \quad (\text{C15})$$

The matrix is diagonal if the deviations are independently distributed (i. e., if $\langle \xi_i \xi_j \rangle = \delta_{ij}$).

a. Covariance matrix for phase

Next, we derive the covariance matrix for the phases. The observations y_i are assumed to have occurred at phases $\phi(t_i, \theta_0) \equiv \phi_i(y(t, \theta_0))$ predicted by the model at the best fit. These phases will differ from the phases ϕ_i calculated from the observations using Eq. (C8) due to the presence of noise in the observations. We define the deviations of the phases as

$$\delta \phi_i \equiv \phi(t_i, \theta) - \phi_i \quad (\text{C16})$$

[see Fig. 9(c)]. These can be related to δy_i by using the functional dependence $\phi_i = \phi_i(y)$ and Eq. (C13):

$$\begin{aligned} \phi_i &= \phi_i(y) \\ &= \phi_i(y(t, \theta) - \delta y) \\ &\approx \phi_i(y(t, \theta)) - \sum_j \frac{\partial \phi_i(y(t, \theta))}{\partial y_j} \delta y_j \\ &= \phi(t_i, \theta) - \sum_j \frac{\partial \phi_i}{\partial y_j} \delta y_j, \end{aligned} \quad (\text{C17})$$

$$\delta \phi_i \approx \sum_j \frac{\partial \phi_i}{\partial y_j} \delta y_j, \quad (\text{C18})$$

where we have kept only the first order terms. This approximation is valid near the best fit where δy_i is small.

At the best fit, we have

$$\delta \phi_i(\theta_0) = - \sum_j \frac{\partial \phi_i}{\partial y_j} \sigma_j \xi_j, \quad (\text{C19})$$

which shows that $\delta \phi_i(\theta_0)$ are random variables with mean 0.

Before proceeding, the derivative $\partial \phi_i / \partial y_j$ merits some attention. First, we note that it may be evaluated using either $y(t_i, \theta)$ or y_i to first order in δy_i :

$$\begin{aligned} \frac{\partial \phi_i(y(t_j, \theta))}{\partial y_j} \delta y_j &= \frac{\partial \phi_i(y_j + \delta y_j)}{\partial y_j} \delta y_j \\ &= \frac{\partial \phi_i(y_j)}{\partial y_j} \delta y_j + O(\delta y^2) \end{aligned} \quad (\text{C20})$$

Second, using Eq. (C8), we can derive an explicit expression for $\partial \phi_i / \partial y_j$:

$$\begin{aligned} \frac{\partial \phi_i}{\partial y_j} &= \frac{\partial}{\partial y_j} \left[\tan^{-1} \left(\frac{H[y]_i}{y_i} \right) \right] \\ &= \frac{1}{1 + (H[y]_i/y_i)^2} \left(\frac{1}{y_i} \frac{\partial H[y]_i}{\partial y_j} - \frac{H[y]_i}{y_i^2} \frac{\partial y_i}{\partial y_j} \right). \end{aligned} \quad (\text{C21})$$

($H[y]_i$ is understood to mean the i th component of the Hilbert transform of y .) To evaluate the derivative $\partial H[y]_i / \partial y_j$, we use the definition of the derivative and the linearity of the Hilbert transform:

$$\begin{aligned} \frac{\partial H[y]_i}{\partial y_j} &= \lim_{h \rightarrow 0} \frac{H[y + h \delta_j]_i - H[y]_i}{h} \\ &= \lim_{h \rightarrow 0} \frac{H[y]_i + h H[\delta_j]_i - H[y]_i}{h} \\ &= H[\delta_j]_i. \end{aligned} \quad (\text{C22})$$

(δ_j is the vector formed by taking the j th column of the Kronecker delta δ_{ij} .) Plugging this into Eq. (C21) gives

$$\frac{\partial \phi_i}{\partial y_j} = \frac{y_i H[\delta_j]_i - H[y]_i \delta_{ij}}{y_i^2 + H[y]_i^2}. \quad (\text{C23})$$

Third, the matrix $\partial \phi / \partial y$ defined by Eq. (C23) is singular (i. e., it has at least one zero eigenvalue). As we now show, this is because changes in the amplitude of an oscillation do not affect the phase.

Theorem. *The matrix $\partial \phi / \partial y$, whose elements are*

$$\frac{\partial \phi_i}{\partial y_j} = \frac{y_i H[\delta_j]_i - H[y]_i \delta_{ij}}{y_i^2 + H[y]_i^2}$$

has at least one zero eigenvalue, corresponding to the eigenvector $\delta y_i^ = y_i$.*

Proof.

$$\begin{aligned}
\sum_j \frac{\partial \phi_i}{\partial y_j} \delta y_j^* &= \sum_j \frac{y_i H[\delta_j]_i - H[y]_i \delta_{ij}}{y_i^2 + H[y]_i^2} y_j \\
&= \frac{y_i H \left[\sum_j \delta_j y_j \right]_i - H[y]_i \sum_j \delta_{ij} y_j}{y_i^2 + H[y]_i^2} \\
&= \frac{y_i H[y]_i - H[y]_i y_i}{y_i^2 + H[y]_i^2} \\
&= 0.
\end{aligned}$$

Any change in amplitude at constant phase is a multiple of y_i and thus also lies in the null space of $\partial \phi / \partial y$.

Returning to Eq. (C18), we derive an expression for the covariance matrix $\Sigma^{\phi(t)}$ for the phases:

$$\begin{aligned}
\Sigma_{ij}^{\phi(t)} &\equiv \langle \delta \phi_i \delta \phi_j \rangle \\
&= \left\langle \sum_k \frac{\partial \phi_i}{\partial y_k} \delta y_k \sum_l \frac{\partial \phi_j}{\partial y_l} \delta y_l \right\rangle \\
&= \sum_{k,l} \frac{\partial \phi_i}{\partial y_k} \langle \delta y_k \delta y_l \rangle \frac{\partial \phi_j}{\partial y_l} \\
&= \sum_{k,l} \frac{\partial \phi_i}{\partial y_k} \Sigma_{kl}^{y(t)} \frac{\partial \phi_j}{\partial y_l}
\end{aligned} \tag{C24}$$

$$\Sigma^{\phi(t)} = \frac{\partial \phi}{\partial y} \Sigma^{y(t)} \frac{\partial \phi^T}{\partial y}. \tag{C25}$$

This shows how the uncertainties in the observations $\sigma_{y_i} = \sqrt{\Sigma_{ii}^{y(t)}}$ are mapped to uncertainties in the phases $\sigma_{\phi_i} = \sqrt{\Sigma_{ii}^{\phi(t)}}$ (see Fig. 10).

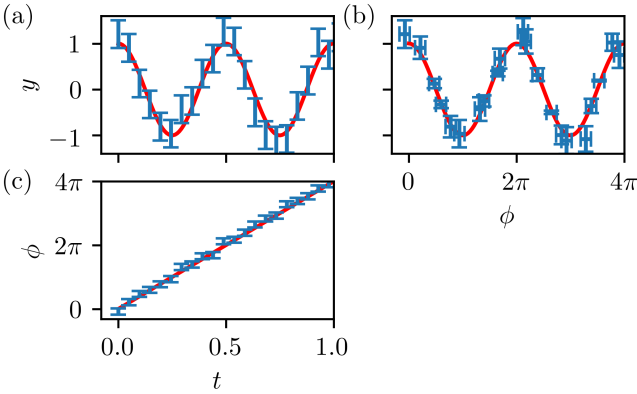


FIG. 10. **Propagation of uncertainty.** (a) Data (blue) simulated from the model $y(t) = A \cos(\omega t)$ (red) by adding uniform Gaussian noise. Error bars indicate uncertainty. (b) Data (blue) plotted as a function of phase compared with $y(\phi) = A \cos(\phi)$ (red). Error bars indicate the uncertainties obtained using Eqs. (C25) and (C31). (c) Phase (blue), obtained for each data point using Eq. (C8), compared with $\phi(t) = \omega t$ (red). Error bars indicate the uncertainties obtained using Eq. (C25).

b. Covariance matrix for observations as a function of phase

Finally, we derive the covariance matrix $\Sigma^{y(\phi)}$ for the observations with phase as the independent variable. We define the deviations of the observations from the predictions at constant phase as

$$\delta \tilde{y}_i \equiv \tilde{y}(\phi_i, \theta) - y_i \tag{C26}$$

[see Fig. 9(b)]. We can relate these to δy_i and $\delta \phi_i$ using Eqs. (C16) and (C10):

$$\begin{aligned}
\delta \tilde{y}_i &= \tilde{y}(\phi_i, \theta) - y_i \\
&= \tilde{y}(\phi(t_i, \theta) - \delta \phi_i, \theta) - y_i \\
&\approx \tilde{y}(\phi(t_i, \theta), \theta) - \frac{\partial \tilde{y}(\phi(t_i, \theta), \theta)}{\partial \phi} \delta \phi_i - y_i \\
&= y(t_i, \theta) - y_i - \left(\frac{\partial \tilde{y}}{\partial \phi} \right)_i \delta \phi_i \\
&= \delta y_i - \left(\frac{\partial \tilde{y}}{\partial \phi} \right)_i \delta \phi_i.
\end{aligned} \tag{C27}$$

In light of Eqs. (C14) and (C19), $\delta \tilde{y}_i$ also has mean 0 at the best fit. Note that, similar to $\partial \phi_i / \partial y_j$, $\partial \tilde{y} / \partial \phi$ may be evaluated using either ϕ_i or $\phi(t_i, \theta)$ to first order in $\delta \phi_i$:

$$\begin{aligned}
\frac{\partial \tilde{y}(\phi(t_i, \theta), \theta)}{\partial \phi} \delta \phi_i &= \frac{\partial \tilde{y}(\phi_i + \delta \phi_i, \theta)}{\partial \phi} \delta \phi_i \\
&= \frac{\partial \tilde{y}(\phi_i, \theta)}{\partial \phi} \delta \phi_i + \mathcal{O}(\delta \phi^2)
\end{aligned} \tag{C28}$$

We can take Eq. (C27) a step further using Eq. (C18):

$$\begin{aligned}
\delta \tilde{y}_i &= \delta y_i - \left(\frac{\partial \tilde{y}}{\partial \phi} \right)_i \delta \phi_i \\
&= \delta y_i - \sum_j \left(\frac{\partial \tilde{y}}{\partial \phi} \right)_i \frac{\partial \phi_i}{\partial y_j} \delta y_j \\
&= \sum_j \left[\delta_{ij} - \left(\frac{\partial \tilde{y}}{\partial \phi} \right)_i \frac{\partial \phi_i}{\partial y_j} \right] \delta y_j \\
&\equiv \sum_j D_{ij} \delta y_j.
\end{aligned} \tag{C29}$$

Taking the expectation of pairs of deviations $\delta \tilde{y}_i$, we obtain

$$\begin{aligned}
\Sigma_{ij}^{y(\phi)} &\equiv \langle \delta \tilde{y}_i \delta \tilde{y}_j \rangle \\
&= \left\langle \sum_k D_{ik} \delta y_k \sum_l D_{jl} \delta y_l \right\rangle \\
&= \sum_{k,l} D_{ik} \langle \delta y_k \delta y_l \rangle D_{jl} \\
&= \sum_{k,l} D_{ik} \Sigma_{kl}^{y(t)} D_{jl}
\end{aligned} \tag{C30}$$

$$\Sigma^{y(\phi)} = D \Sigma^{y(t)} D^T. \tag{C31}$$

This gives us a way to compute the uncertainties of the observations $\sigma_{\tilde{y}_i} = \sqrt{\Sigma_{ii}^{y(\phi)}}$ when taking phase as the independent variable instead of time (see Fig. 10).

3. New cost using phase

Our new cost is motivated by Eq. (C27); rearranging it, we have

$$\delta y_i \approx \delta \tilde{y}_i + \left(\frac{\partial \tilde{y}}{\partial \phi} \right)_i \delta \phi_i. \quad (\text{C32})$$

This relation constitutes a first order approximation of the deviations δy_i that decouples changes in phase or frequency from changes in amplitude. Because this approximation includes only first order terms in $\delta \phi_i$, it eliminates the nonlinear dependence on frequency that results in ripples in the cost [refer to Eq. (C4) and Fig. 9]. In fact, if we substitute this into Eq. (C2), we obtain a quadratic approximation of the cost near the best fit:

$$C^{y(t)} = \frac{1}{2} \sum_{i,j} \delta y_i \left(\Sigma^{y(t)} \right)_{ij}^{-1} \delta y_j \quad (\text{C2})$$

$$\approx \frac{1}{2} \sum_{i,j} \left[\delta \tilde{y}_i + \left(\frac{\partial \tilde{y}}{\partial \phi} \right)_i \delta \phi_i \right] \left(\Sigma^{y(t)} \right)_{ij}^{-1} \times \left[\delta \tilde{y}_j + \left(\frac{\partial \tilde{y}}{\partial \phi} \right)_j \delta \phi_j \right] \quad (\text{C33})$$

We use Eq. (C33) to define the new cost for oscillatory systems:

$$C^\phi \equiv \frac{1}{2} \sum_{i,j} \left[\delta \tilde{y}_i + \left(\frac{\partial \tilde{y}}{\partial \phi} \right)_i \delta \phi_i \right] \left(\Sigma^{y(t)} \right)_{ij}^{-1} \times \left[\delta \tilde{y}_j + \left(\frac{\partial \tilde{y}}{\partial \phi} \right)_j \delta \phi_j \right] \quad (\text{C34})$$

This definition accounts for both differences between observations and predictions at constant phase and differences in the phases of the observations and predictions. It may be decomposed into three pieces:

$$C^\phi = C^{\tilde{y}(\phi)} + C^X + C^{\phi(t)} \quad (\text{C34a})$$

$$C^{\tilde{y}(\phi)} \equiv \frac{1}{2} \sum_{i,j} \delta \tilde{y}_i \left(\Sigma^{y(t)} \right)_{ij}^{-1} \delta \tilde{y}_j \quad (\text{C34b})$$

$$C^X \equiv \frac{1}{2} \sum_{i,j} \delta \tilde{y}_i \left(\Sigma^{y(t)} \right)_{ij}^{-1} \left(\frac{\partial \tilde{y}}{\partial \phi} \right)_j \delta \phi_j + \frac{1}{2} \sum_{i,j} \left(\frac{\partial \tilde{y}}{\partial \phi} \right)_i \delta \phi_i \left(\Sigma^{y(t)} \right)_{ij}^{-1} \delta \tilde{y}_j \quad (\text{C34c})$$

$$C^{\phi(t)} \equiv \frac{1}{2} \sum_{i,j} \left(\frac{\partial \tilde{y}}{\partial \phi} \right)_i \delta \phi_i \left(\Sigma^{y(t)} \right)_{ij}^{-1} \left(\frac{\partial \tilde{y}}{\partial \phi} \right)_j \delta \phi_j. \quad (\text{C34d})$$

We compare $C^{y(t)}$, $C^{\tilde{y}(\phi)}$, $C^{\phi(t)}$, and C^ϕ in Fig. 11.

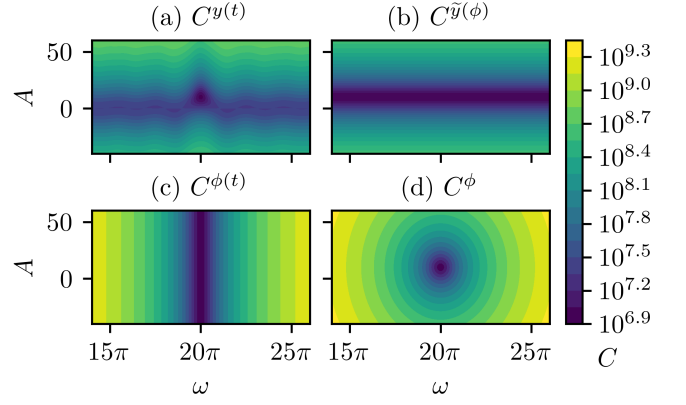


FIG. 11. **Cost decomposition** of the model $y(t) = A \cos(\omega t)$. (a) Same as Fig. 8. (b) $\tilde{y}(\phi) = A \cos(\phi)$ is insensitive to changes in frequency. (c) $\phi(t) = \omega t$ is insensitive to changes in amplitude. (d) Cost using Eq. (C34). The ripples have been replaced with a quadratic basin.

4. Fisher Information Matrix (FIM)

In general, the FIM is related to the cost by

$$I_{\mu\nu} = \left\langle \frac{\partial^2 C(\theta_0)}{\partial \theta_\mu \partial \theta_\nu} \right\rangle. \quad (\text{C35})$$

Given that $\langle \delta y_i(\theta_0) \rangle = 0$, this leads to Eq. (C3) for the cost in Eq. (C2). We have already shown that $\langle \delta \phi_i(\theta_0) \rangle = 0$ and $\langle \delta \tilde{y}_i(\theta_0) \rangle = 0$. Accordingly, applying Eq. (C35) to the new cost [Eq. (C34)] gives

$$I_{\mu\nu} = \sum_{i,j} \left(\frac{\partial \tilde{y}}{\partial \phi} \right)_i \frac{\partial \phi_i}{\partial \theta_\mu} \left(\Sigma^{y(t)} \right)_{ij}^{-1} \left(\frac{\partial \tilde{y}}{\partial \phi} \right)_j \frac{\partial \phi_j}{\partial \theta_\nu} + \sum_{i,j} \left(\frac{\partial \tilde{y}}{\partial \phi} \right)_i \frac{\partial \phi_i}{\partial \theta_\mu} \left(\Sigma^{y(t)} \right)_{ij}^{-1} \frac{\partial \tilde{y}_j}{\partial \theta_\nu} + \sum_{i,j} \frac{\partial \tilde{y}_i}{\partial \theta_\mu} \left(\Sigma^{y(t)} \right)_{ij}^{-1} \left(\frac{\partial \tilde{y}}{\partial \phi} \right)_j \frac{\partial \phi_j}{\partial \theta_\nu} + \sum_{i,j} \frac{\partial \tilde{y}_i}{\partial \theta_\mu} \left(\Sigma^{y(t)} \right)_{ij}^{-1} \frac{\partial \tilde{y}_j}{\partial \theta_\nu}. \quad (\text{C36})$$

We have assumed $\Sigma^{y(t)}$ is symmetric.

We now show that Eq. (C36) is equivalent to Eq. (C3). First, recall Eq. (C10),

$$y(t, \theta) = \tilde{y}(\phi(t, \theta), \theta), \quad (\text{C37})$$

and differentiate it with respect to θ_μ :

$$\frac{\partial y}{\partial \theta_\mu} = \frac{\partial \tilde{y}}{\partial \phi} \frac{\partial \phi}{\partial \theta_\mu} + \frac{\partial \tilde{y}}{\partial \theta_\mu}. \quad (\text{C38})$$

This relationship is exact and shows a decoupling of the amplitude sensitivity from the phase sensitivity, similar to Eq. (B5). Substituting Eq. (C38) into Eq. (C3) results in Eq. (C36) (q.e.d.). Because the FIM is preserved, the new cost [Eq. (C34)] constitutes an isometric embedding of the model manifold.

5. Parameter sensitivities

Eq. (C8) may be differentiated to obtain both first- and second-order parameter sensitivities. Using Eq. (C7), denoting $\partial_\mu \equiv \partial/\partial\theta_\mu$, and assuming the Hilbert transform commutes with ∂_μ , we obtain (dropping explicit functional dependencies after the first line for clarity):

$$\phi(t, \theta) = \tan^{-1} \left(\frac{H[y](t, \theta)}{y(t, \theta)} \right) \quad (C39)$$

$$\partial_\nu \phi = \frac{1}{A^2} (H[\partial_\nu y] y - H[y] \partial_\nu y) \quad (C40)$$

$$\begin{aligned} \partial_\mu \partial_\nu \phi = & \frac{2}{A^4} (y \partial_\mu y + H[y] H[\partial_\mu y]) (H[y] \partial_\nu y - H[\partial_\nu y] y) \\ & + \frac{1}{A^2} (H[\partial_\nu y] \partial_\mu y - H[\partial_\mu y] \partial_\nu y \\ & + H[\partial_\mu \partial_\nu y] y - H[y] \partial_\mu \partial_\nu y). \end{aligned} \quad (C41)$$

The first-order sensitivities for \tilde{y} can be obtained by rearranging Eq. (C38):

$$\partial_\mu \tilde{y} = \partial_\mu y - \frac{\partial \tilde{y}}{\partial \phi} \partial_\mu \phi. \quad (C42)$$

Differentiating Eq. (C38) a second time and rearranging yields the second-order sensitivities:

$$\begin{aligned} \partial_\mu \partial_\nu \tilde{y} = & \partial_\mu \partial_\nu y - \frac{\partial}{\partial \phi} (\partial_\nu \tilde{y}) \partial_\mu \phi - \frac{\partial}{\partial \phi} (\partial_\mu \tilde{y}) \partial_\nu \phi \\ & - \frac{\partial^2 \tilde{y}}{\partial \phi^2} \partial_\mu \phi \partial_\nu \phi - \frac{\partial \tilde{y}}{\partial \phi} \partial_\mu \partial_\nu \phi. \end{aligned} \quad (C43)$$

6. Alternatives for obtaining a phase

In some cases, Eq. (C8) cannot be used to obtain a monotonically increasing phase. For example, some oscillatory behavior does not have a single center of oscillation. If that is the case, one approach is to decompose the signal using *empirical mode decomposition* into a number of *intrinsic mode functions*, for each of which a separate phase may then be defined [60]. However, because this method is empirical, the decomposition may not vary smoothly with the parameters of the model, leading to discontinuities in the cost function.

Even when the oscillatory behavior does have a single center of oscillation, in practice the Hilbert transform must be implemented numerically. This usually involves a fast Fourier transform, which can introduce unwanted

effects in the phase due to the Gibbs phenomenon (see Fig. 12). The impact of end effects can be reduced by leaving the ends out of the cost function, or through windowing.

More generally, any monotonically increasing function of time may be used for a phase, provided it has the appropriate frequency. Thus, one proposal is to use

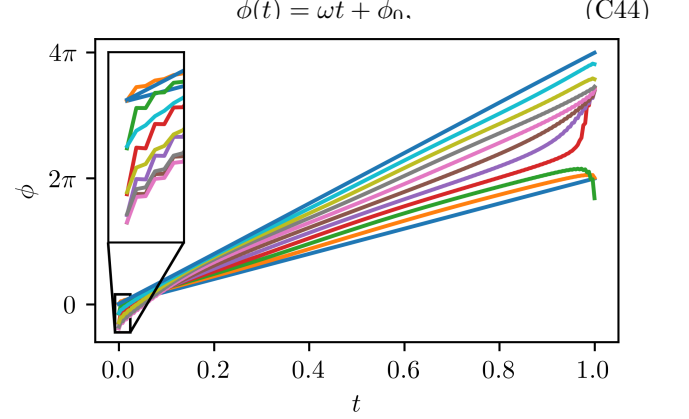


FIG. 12. Phases obtained when implementing the Hilbert transform numerically on the model $y(t, \theta) = A \cos(\omega t)$, for ω ranging from 2π to 4π . The effects of the Gibbs phenomenon can be seen near the ends for some values of ω .

and to estimate a value of ω from the oscillatory signal. This may be done by fitting a line to the phase obtained from Eq. (C8), or by using a Fourier transform to decompose the signal into frequency components and selecting one (perhaps the lowest).

We also suggest the following method of obtaining a phase that does not require the use of the Hilbert transform [37]. It is sometimes the case that two signals, $y_1(t)$ and $y_2(t)$, can be selected from the dynamical variables $y(t)$ of a system and used to calculate a phase as follows:

$$\phi(t) = \arctan \left(\frac{y_2(t)}{y_1(t)} \right). \quad (C45)$$

The only requirement is that the combined signal correspond to a *proper rotation*, which has both a definite direction and unique center of rotation, so that the phase will be monotonically increasing [59, 61]. For example, in some cases, a signal $y(t)$ and its time derivative $\dot{y}(t)$ may be used:

$$\phi(t) = \arctan \left(\frac{y(t)}{\dot{y}(t)} \right). \quad (C46)$$